Chaos, Solitons and Fractals 165 (2022) 112874

Contents lists available at ScienceDirect

Chaos, Solitons and Fractals

journal homepage: www.elsevier.com/locate/chaos

Review

Information theory and earthquakes: Depth propagation seismicity in northern Chile

Denisse Pasten [a,*], Gonzalo Saravia [b], Eugenio E. Vogel [c,d], Antonio Posadas [e,f]

[a] Departamento de Física, Facultad de Ciencias, Universidad de Chile, Santiago, Chile
[b] Los Eucaliptus 1189, Temuco 4812537, Chile
[c] Departamento de Ciencias Físicas, Universidad de La Frontera, Temuco, Chile
[d] Center for Nanoscience and Nanotechnology, Santiago, Chile
[e] Instituto Andaluz de Geofísica, Campus Universitario de Cartuja, Universidad de Granada, 18071 Granada, Spain
[f] Departamento de Química y Física, Universidad de Almería, 04120 Almería, Spain

ARTICLE INFO

Keywords:
Mutability
Non-linear phenomena
Earthquakes
Information theory

ABSTRACT

Mutability is an information theory tool intended to characterize sequences of non-linear phenomena (e.g., earthquakes). In this study, we used mutability to identify and analyze the depth propagation of seismicity in northern Chile. During March/April 2014, several important earthquakes struck northern Chile, including one of magnitude 8.1, producing intense but short-lived aftershock regimes. To better understand this behavior, we used data from the Integrated Plate Boundary Observatory Chile (IPOC) catalog. In a first approach, we considered 101,601 earthquakes registered from January 1, 2007 to December 31, 2014 within a rectangle defined by the coordinates 68 W–72 W and 18S—22S. Based on Gutenberg–Richter analysis, earthquakes with magnitudes of >2.3 (a subset of 79,321 seisms) were selected for further analysis and were grouped by depth into overlapping bins in order to identify the depth propagation of the aftershock regimes. The largest two March 2014 earthquakes produced responses from near the surface to ~18 km depth. The largest two early April earthquakes had deeper aftershock regimes. In addition, using static information theory, we performed a detailed layer-by-layer analysis that shows that the March 2014 activity had larger response towards the surface, while the April 2014 activity showed larger activity towards the inner layers. To reach more recent years data from Centro Sismológico Nacional (CSN) covering from 2012 to the end of 2021 as used. The results show a similarity between the mutability and dynamic average depths of seismicity from 2012 to 2021. The mutability of recent years is slightly less than the historic average, which can be interpreted to reflect relaxing mechanisms that are postponing the expected megathrust event in this zone.

1. Introduction

Emergent phenomena can be found in natural systems such as the magnetosphere [1], fluid turbulence [2], climate [3], and seismicity [4]. The complexity of natural phenomena involves the conjugation of different events and the evolution of these events in time. The occurrence of a large earthquake unites a series of elements that bring the system to a critical point, for which the mechanics are known. However, the periodicity or migration of aftershocks cannot be known in advance; even the areas of highest aftershock activity cannot be predicted. The presence of emergent phenomena is crucial for better identifying the mechanisms through which large seismic events and subsequent seismicity are generated. However, while the physical effects of large earthquakes are evident and measurable (e.g., damage to infrastructure, changes in geography and the landscape), the impact of an earthquake at depth is not easy to analyze.

Information theory has been used in the analysis of earthquake occurrence in different zones of the planet. Telesca et al. have studied the inter-event time of seismic events through Shannon entropy and/or Fisher information measure in different places of the Earth [5–8]. In a recent work they show how information theory can five lights about how water reservoirs can trigger earthquakes in Vietnam, for example [9]. On the other hand, Varotsos et al. have extensively studied the concept of natural time in time sequences of slight earthquakes occurred between two large earthquakes [10–14]. To these methods now we can add the nowcasting method developed recently by Rundle et al. in 2018

* Corresponding author.
E-mail addresses: denissepasten@uchile.cl (D. Pasten), eugenio.vogel@ufrontera.cl (E.E. Vogel), aposadas@ual.es (A. Posadas).

https://doi.org/10.1016/j.chaos.2022.112874
Received 15 July 2022; Received in revised form 29 September 2022; Accepted 1 November 2022
Available online 16 November 2022

and 2019 [15,16]. This method tries to give a classification of the seismic risk in a specific region based on the idea of the seismic cycle. Thereby, using the concept of Shannon Information Theory, they carry out an analysis considering the information entropy over frequency-magnitudes. Although the latter provides similar information to that already obtained by natural time, it returns to the information entropy as a useful hypothesis to address the seismic hazard in certain areas of the planet. As explained in the Methodology Section below we use here an alternative way of dealing with information theory, with connections to Shannon entropy.

On 1 April 2014, after a series of early precursors [17–19], a Mw 8.1 earthquake occurred near the city of Iquique, northern Chile. This area is of particular research interest owing to a seismic gap between southern Peru and northern Chile since the last mega-earthquake, a devastating Mw 8.5 event in 1877 [20]. During the last three decades, several events of magnitude >Mw 7.0 had occurred in this region [19,21,22]. However, various studies have highlighted the potential risk for a larger earthquake in this region, including those of Ruiz et al. [18], León-Ríos et al. [23], and Ruiz and Madariaga [20]. In 2006, in response to increased seismic activity, the Integrated Plate Boundary Observatory Chile (IPOC) network was installed in northern Chile to systematically record seismic activity in this region. However, subsequent seismic activity did not behave as anticipated. High seismic activity before the earthquake of April 1 lead to speculation that a megathrust event would occur in this seismic gap. However, the seismic events of March and April of 2014 only ruptured a zone of low coupling; they did not extend to the entire seismic gap as expected. To better understand this behavior, we investigated the effects of the 2014 earthquakes at different depths and compared the results with previous activity in the area from 2007 to 2014.

Using data from the IPOC catalog for northern Chile [24], we focused our analyses on plate interface seismicity, for which the catalog contains 9818 earthquakes. In addition, in order to include more recent seismic data in our analyses, we also used the Centro Sismológico Nacional (CSN) catalog (https://doi.org/10.7914/SN/C1), which contains 22,248 seismic events in northern Chile between 2012 and 2021. Data analysis was performed by combining basic statistics with information theory techniques. In particular, we applied the concept of mutability to

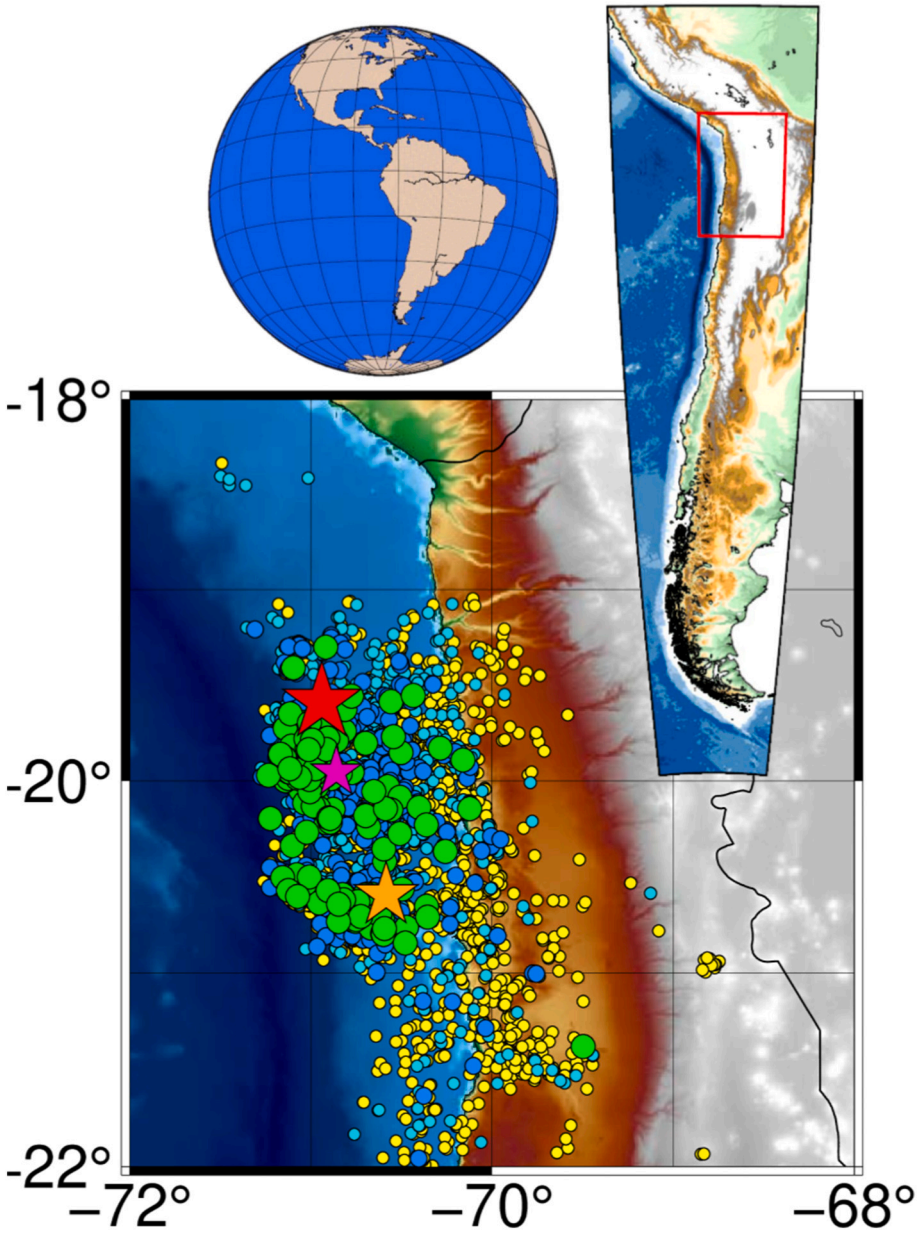

Fig. 1. Seismicity within a rectangle defined by the coordinates 68 W–72 W and 18S—22S (i.e., northern Chile) during 2014. The red star denotes the Mw8.1 Iquique earthquake of April 12,014; the orange star denotes the Mw7.6 aftershock of April 32,014; the magenta star denotes the Mw6.6 foreshock of March 16, 2014. Yellow circles denote earthquakes of $2.0 \leq M \leq 2.9$, cyan circles denote earthquakes of $3.0 \leq M \leq 3.9$, blue circles denote earthquakes of $4.0 \leq M \leq 4.9$, and green circles denote earthquakes of $5.0 \leq M \leq 6.5$. (For interpretation of the references to colour in this figure legend, the reader is referred to the web version of this article.)

detect differences in the responses to earthquakes at different depths. Mutability has previously been used in seismology [25,26] as well as in other fields as discussed below [27–36].

2. Geological context

The subduction zone of northern Chile is formed by the subduction of the Nazca Plate beneath the South American Plate at a rate of ~6–7 cm per year. Large historical earthquakes in northern Chile occurred in 1543, 1615, 1786, and 1877 [20]. The last mega-earthquake, which occurred on May 9, 1877, had a magnitude of >Mw 8.5; it caused a rupture of ~500 km in length and generated a devastating tsunami that affected the coast from Arica to the Mejillones Peninsula. A number of subsequent earthquakes of magnitude >7.0 have occurred (i.e., the 1911 Mw 7.1 Iquique earthquake, 1933 Mw7.6 Iquique earthquake, 1940 Mw 7.10 Iquique earthquake, 1967 Mw7.4 Tocopilla earthquake, 1995 Mw 8.0 Antofagasta earthquake [21], 2001 Mw8.4 Arequipa earthquake [22], and 2007 Mw7.7 Tocopilla earthquake [19]). However, large sections of the1877 rupture have not been ruptured since. As such, northern Chile and southern Peru represent a seismic gap, within which a large earthquake has been expected for many years [20,37,38].

The rupture of the 2014 Mw8.1 Iquique earthquake, which struck on April 1, 2014, was ~200 km in length [23] and only broke a low coupling region [37,38] in the central zone of the seismic gap (Fig. 1). Prior to the earthquake, seismic activity in the region had been increasing since 2008, culminating in foreshocks of Mw 6.6 and 6.4 on March 16 and March 17, 2014, two weeks before the mainshock. Among a series of aftershocks, the most significant occurred 100 km to the south of the mainshock on April 3, 2014, with a magnitude of Mw 7.6. Ruiz et al. [39] concluded that seismicity associated with the Mw 8.1 event was mainly distributed around the trench to the southwest of the rupture zone, with foreshocks and aftershocks principally located on the shallow interplate interface.

3. Methodology

3.1. Selection and treatment of the relevant data

In this study, we focused on seismicity within the epicentral zone of the 2014 Iquique earthquake (Table 1), which was defined by a rectangle formed by the coordinates 68 W–72 W and 18S—22S as illustrated in Fig. 1. Since this is the only rectangle over which data was collected, we will not repeat this information in the rest of the text or the plots. Most of the present study makes use of the data from the very accurate IPOC catalog to investigate seismicity on the plate interface [24]. The IPOC network was installed in 2006 to monitor seismic activity in northern Chile, including that in the seismic gap. The network was created as an association between the University of Chile, GeoForschungsZentrum (GFZ) of Germany, and the Institut de Physique du Globe de Paris (IPGP) in France [24]. It consists of 20 sites equipped with broadband seismometers, accelerometers, and double frequency Global Positioning System (GPS) receivers. The IPOC catalog for northern Chile [24] contains 101,601 seismic events recorded between 2007 and 2014. In addition, in order to extend part of our analyses to more recent years (for which IPOC data are not available), we also extracted data from the CSN catalog (https://doi.org/10.7914/SN/C1), which contains 22,248 seismic events between January 1, 2012 and December 31, 2021 for the same rectangular region. Although not entirely equivalent to that of the IPOC, the CSN catalog provides a good description of seismic activity in the region until recently.

Table 1
Earthquakes of magnitude Mw6.3 and higher within a rectangle defined by the coordinates 68 W–72 W and 18S—22S (see Fig. 1). Four reference seismic events (a triggering earthquake and the next important in magnitude) are highlighted in boldface. The earthquakes of April 3 were separated by 45 min. The March 22 earthquake occurred at a depth nearly twice that of the other events, with the hypocenter well inside the Nazca plate.

Date (yyyy-mm-dd)	Magnitude	Latitude	Longitude	Depth (km)
2014-03-16	**6.6**	**−19.95476**	**−70.85965**	**17.86**
2014-03-17	**6.4**	**−19,97,812**	**−70.95194**	**21.09**
2014-03-22	6.3	−19.74193	−71.03003	46.32
2014-04-01	**8.1**	**−19.58927**	**−70.94021**	**19.91**
2014-04-03	6.4	−20.23952	−70.68120	24.34
2014-04-03	**7.6**	**−20.59462**	**−70.58543**	**21.96**
2014-04-04	6.3	−20.59444	−70.70383	22.50
2014-04-11	6.3	−20.70646	−70.72461	20.72

3.2. Analysis and algorithms

We first analyzed the data using simple statistics, and then applied the wlzip recognizer to the time lags in the earthquake sequences. A similar approach has been used in past studies [25,26], which is now improved in the tuning possibilities of digits recognitions in the way explained a few paragraphs below.

There are three reasons to use time lags between consecutive earthquakes as the observable on which perform the information recognition: i) Time lags between consecutive earthquakes span three orders of magnitude allowing to recognize different regimes; ii) Mutability can be tuned to the significant digits in the time lags sequence bearing the more relevant information; iii) Differences in time among different stations is usually negligible as compared to differences in magnitude or depth. As for the definition this is simply given by the time difference (in minutes is OK) between consecutive seisms over a critical magnitude and within the geographical area of interest. We can further define average time lags, standard deviations for the sequence, mutability, and other statistical variables or indicators. A detailed description of this approach can be found in Vogel et al. [25]. In brief, wlzip uses data compressor techniques to recognize digits for records of an equal number of digits along a vector file.

Among the variables produced by a seismic data sequence it is the time lags or time intervals among consecutive sequence the one that spans more orders of magnitude. The first task is to produce files with the time intervals δ in minutes between consecutive earthquakes. Then, we invoke a data recognizer like wlzip to search for repeated registers and produces a new file with a map of previous one. We briefly review here the method which has been developed.

It originated in dealing with sequences of data for magnetic systems: Monte Carlo simulations provide sequences of magnetization or any order parameter for each separate temperature, after equilibration [27–29]. The weight in bytes for such file is w. Then wlzip produces a map of previous file recognizing repetitions using algorithms similar to those of data compression; the weight of the "compressed" file is w^*. The more and sooner the same register repeats itself along the data chain, the shorter the new file becomes.

In this way we have two data chains: the mutability μ for this series is defined as the ratio:

$$\mu = \frac{w^*}{w}. \tag{1}$$

This definition can apply to the whole file or to windows along the file in a dynamic process that produces a function $\mu_\nu(t)$, where the recognition considers a window of the ν registers ending at the instant t. The number of elements ν appropriate to a given problem must be searched in each application of the technique. For the present application, we found that $\nu = 64$ produced results that enhance the aftershock regime. This can be appreciated in Fig. A1 of the Appendix.

Previous definition applies to any data sequence, so this method was later successfully applied to fields beyond magnetism: econophysics [30,31], blood pressure [32,33], polymer deposition [34,36], wind energy generation [35] and earthquake recognition [25,26]. It is precisely

in these last two papers where details of the application of this method to seismic data has been explained in detail. We briefly summarize here some technical elements relevant to the present study.

Data recognition can be achieved by looking at the whole register (including noise) or at the most sensitive digits bearing the most important variation in the data. To accomplish this task, all registers must have the same number of digits. Suppose one such register is 01432, namely an interval of 1432 min between two consecutive earthquakes. The leading zero is needed so that all registers have 5 digits. Depending on the sequence it can be convenient to focus the recognition on some of the positions denoted by *(i,r)*, where *i* identifies the position of the first digit under consideration and *r* gives the range or number of positions recognized from there to the right. Thus, (1,5) means recognition of the five digits; (2,3) means recognition of digits in the second, third, and fourth positions (e.g., digits 1, 4 and 3 in the example); (3,2) means recognition of the third and fourth digits only (e.g., digits 4 and 3 in the example). A larger range for the mutability (i.e., better characterization of extreme behaviors) is obtained when *(i,r)* determines the most sensitive digit positions for the data under consideration. Therefore, this is a calibration process that needs to be performed specifically for each problem. We tested all possible *(i,r)* combinations and identified a truncation of (2,3) as the most appropriate for the present application. Appendix 1 presents a plot for the series *(i,3)*, illustrating how (2,3) was picked for the present work.

Mutability has no absolute meaning and can only be used for relative comparisons within a sequence. Generally speaking, low values of μ indicate calm periods for the variable, while high values mean the opposite, namely rapidly changing values of that variable along that part of the sequence. Thus, aftershock periods have low mutability values due to successions of short time lags most of which presenting 2 or 3 zeros as the leading 5 digits, so producing many numerical coincidences.

With all the seisms in this database we conducted a statistical analysis in which the distribution of earthquake magnitudes follows an empirical and universal relationship, usually called the Gutenberg-Richter relationship (GRr) [40]:

$$log n(M >) = a - bM \tag{2}$$

where $n(M >)$ is the cumulative number of earthquakes with magnitude equal to or larger than M, and a and b are real constants that may vary in space and time. Parameter a characterises the general level of seismicity in a given area during the study period (i.e., the higher the a value, the higher the seismicity), whereas parameter b, which is typically close to 1, describes the relative abundance of large to smaller shocks. The idea is to determine M_C the threshold value over which the linear behavior holds ensuring a normal distribution.

Although some studies estimate the value of M_C by fitting GRr to the observed frequency–magnitude distribution (the magnitude at which the lower end of the frequency–magnitude distribution departs from the GRr is taken as an estimate of M_C) [41], there are several other methods to better determine the threshold magnitude (M_C). Catalog-based techniques include day-to-night noise modulation (the day/night method) [42], M_C from the Entire Magnitude Range [43], the maximum curvature technique (MAXC) [44], the M_C by b-value stability (MBS) approach [45], and median-based analysis of the segment slope (MBASS) [46]. The maximum curvature technique is mainly used in applied techniques and was chosen here; however, the results do not differ significantly among these approaches. The Gutenberg–Richter relationship is shown in Fig. 2 and the MAXC technique indicated that $M_C \approx 2.3$. We plotted magnitude vs. time in Fig. 3 to visualize the seismic energy released in the area of interest and the period from January 2014 to April 2014.

There are two main classes of methods to evaluate M0 [47]: catalog-based methods (e.g., Rydelek and Sacks [48], Woessner and Wiemer [49], and Amorèse [50]) and network-based methods (e.g., Kvaerna and Ringdal [51], Schorlemmer and Woessner [52], D'Alessandro et al. [53]). We used a catalog-based method because the necessary inputs were available from our dataset. Although some studies estimate the value of M_0 by fitting GRr to the observed frequency-magnitude distribution (the magnitude at which the lower end of the frequency-magnitude distribution departs from the GRr is taken as an estimate of M_0) [54], there are several other methods that can help us to a better determine the threshold magnitude. Some of the catalog-based techniques include the day-to-night noise modulation (day/night method) [48], the M_0 from the Entire Magnitude Range [55], the MAXC technique [40], the Goodness-of-Fit Test (GFT) [40], the M_0 by b-value stability (MBS) approach [56], and the Median-based analysis of the segment slope (MBASS) [50]. The maximum curvature technique is mainly used in applied techniques and was chosen here; however, the results do not differ significantly among these approaches. The Gutenberg–Richter relationship is shown in Fig. 2 and the MAXC technique indicated that $M_C \approx 2.3$. We plotted magnitude vs. time to visualize the seismic energy released in the area and period selected (Fig. 3a); a detailed plot of the period from January 2014 to April 2014 (Fig. 3b) was used to define the series A, series B, and series C subsets (see Section 3a for details).

Major earthquakes and aftershocks usually occur at the subduction front. As such, we focused on earthquakes produced at depths of 6–52

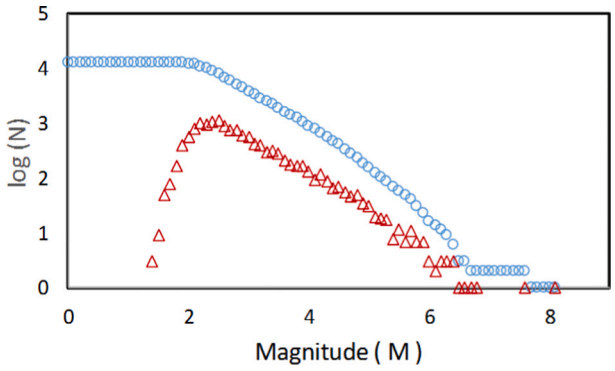

Fig. 2. Guttenberg–Richter analysis of seismicity in northern Chile during 2014 for the area of interest. Red triangles denote the numbers of events in each magnitude bin and blue circles denote the cumulative frequency–magnitude distributions of events. From the maximum curvature (MAXC) technique, the threshold magnitude (M_C) for catalog completeness is M = 2.3. (For interpretation of the references to colour in this figure legend, the reader is referred to the web version of this article.)

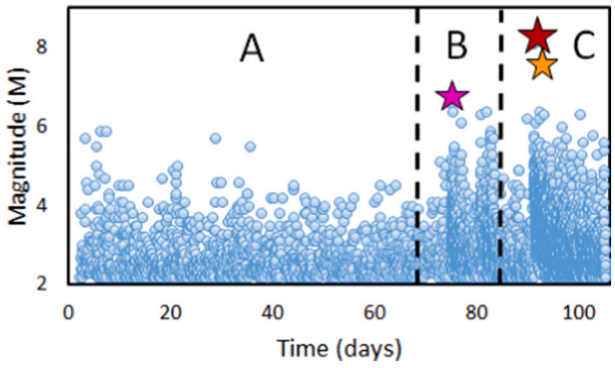

Fig. 3. Magnitude vs. time (in days) for seismicity in the defined rectangle, from January 1 to April 16, 2014, split into series A (January 1 to March 15), series B (March 16 to March 31), and series C (April 1 to April 16). The red star denotes the Mw8.1 earthquake of April 1, 2014, the orange star denotes the Mw 7.6 earthquake of April 3, 2014, and the magenta star denotes the Mw6.6 earthquake of March 16, 2014. (For interpretation of the references to colour in this figure legend, the reader is referred to the web version of this article.)

km; surface events, which are not related to subduction, were excluded. The lower limit of 52 km was arbitrary; choosing other similar depths yielded similar results. We classified events by depth using overlapping bins of 6–12, 9–15, 12–18, 15–21, 18–24, 21–27, 24–32, 28–36, 32–40, 36–44, 40–48, and 44–52 km. The overlap was intended to compensate for layers with low activity and to maximize the probability of having a triggering earthquake and most of its aftershocks within the same layer.

4. Results and discussion

Fig. 4 shows the mutability of δ for the earthquakes of 2007–2014. For the most part, its value is between 0.6 and 0.8; however, near event 48,000, the mutability function experienced a sudden and oscillatory decrease in the form of needles pointing downwards but, indicating a rapid succession of repetitive values of δ. This feature is indicative of an aftershock regime. To better understand the aftershock responses, we divide the year 2014 in 4-time intervals each one with its associated series of seisms. (1) Series A, extending from January 1 to March 15, 2014, when the first triggering event occurred (see Table 1): there were no large earthquakes or aftershocks and mutability oscillated around 0.7. (2) Series B, lasting 16 days from March 16 to March 31, 2014 (just before the second triggering event and largest earthquake occurred), during which there were at least two important earthquakes (Mw 6.6 and 6.4) and associated aftershock responses; during this time, mutability fell to almost 0.3. (3) Series C, extending for 16 days (so it is the same previous time span) from April 1 to April 16, 2014, during which there were two major earthquakes (including the largest event of Mw 8.1); this period saw the superposition of the remaining of the previous aftershock regime and the vigorous new one with mutability reaching just under 0.15. (4) Series D, extending from there to the end of 2014, when no major earthquakes occurred, and mutability steadily recovered in an oscillatory manner to a value of just under 0.7. The four significant earthquakes listed in Table I, which occurred during series B and C, led to different aftershock regimes, with the strongest event (Mw 8.1 on April 1, 2014) producing the most pronounced fall in mutability.

Fig. 5 shows a statistic analysis of earthquake properties. In terms of number of events (Fig. 5a), series A had very low activity overall, with slightly more earthquakes at intermediate depths, serving as a reference of the activity just before a great seism. During series B, the number of events increased until ~28 km depth, below which activity was low (similar to that of Series A). During series C, which included the largest event, the numbers of events were the highest, increasing until 28 km and then decreasing with increasing depth. This uneven number of seisms with depth was the reason to prepare wider bins over 28 km to allow for better statistics.

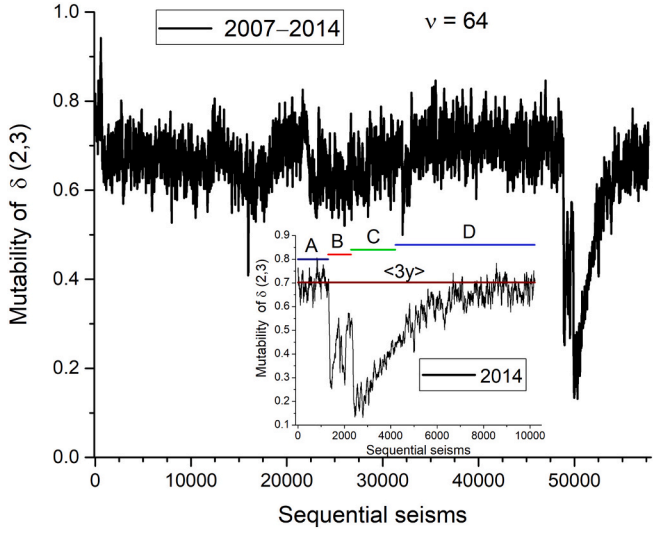

Fig. 4. Mutability of the sequence for δ from 2007 to 2014. The intense activity of 2014 is displayed in the inset, in which the horizontal line labeled ⟨3y⟩ represents the average value of the mutability function for the previous 3 years of the full period (2011, 2012, and 2013) and the colored bars represent series A, B, C, and D. Note that the sequence of earthquakes (x axis) is not linear with time.

In terms of average magnitude (Fig. 5b), during series A, the largest events were at intermediate depths (~15–27 km) while the lowest average magnitude was at ~32 km (the point at which the number of earthquakes was also at a minimum); series B and C show similar patterns. The average magnitudes all occur within $3.0 \leq M \leq 3.6$; as such, magnitude does not offer a distinctive characteristic to distinguish the different series.

To display the important differences in intervals δ between consecutive seismic events, the logarithm of ⟨δ⟩ was plotted on the y axis (Fig. 5c). Using these differences, we can discriminate between series and between different depths within a given series. For this reason, we focused on δ for our subsequent analyses. The mutability curves for the δ sequences (Fig. 5d) are also illustrative because of the different activity developed under dissimilar conditions. The values for series A, which had a small number of events, remained high regardless of depth. For series B, mutability fell as the depth increased to 21–27 km depth, after which it increased again. Series C showed a similar pattern but fell to even smaller values at depths of 21–32 km. Down to 27 km, series C likely contains a contribution from the sequence triggered by the March 16 earthquake (which occurred during series B). We prepared figures with all bins of 6 km similar to those presented in Fig. 5: the tendency is the same, but some dispersion is noticed for the deeper bins because of poorer statistics.

Fig. 6 shows the detailed variations in mutability within different depth intervals. Owing to the limited number of earthquakes involved in each plot, direct comparisons among several depths was not possible; however, a number of observations can still be made. First, the number of induced earthquakes decreases with depth, as demonstrated by the larger gap between stars representing the March earthquakes in the 12–18 km interval compared with the 18–24 km interval. This is corroborated by the relative values of the first drop in mutability, which is larger for the 12–18 km interval (Fig. 6a) than for the 24–32 km interval (Fig. 6c). The second drop in mutability is smaller than the first within the 12–18 km depth interval (Fig. 6a), approximately equal to the first in the 18–24 km depth interval (Fig. 6b), and clearly dominates in the 24–32 km depth interval (Fig. 6c). The recovery of mutability to values similar to those before 2014 is achieved at shallow depths but not at larger depths. Finally, aftershock activity generated by a 2009 earthquake (hypocenter: 19.659S, 70.731 W; depth: 27.2 km; magnitude 6.2) is clear after ~100 earthquakes at 24–32 km depth (Fig. 6c).

Fig. 6a, b, and d all show the recovery of mutability values after the main seismic activity during 2014. However, between 24 and 32 km (Fig. 6c), mutability does not show a complete recovery. The results shown in Fig. 6d remain unexplained. We observed high mutability at 32–40 km depth up to event ~800 (the Mw 8.1 earthquake), with no evidence for the 2009 event, which is marked by a low mutability spike in the previous layer (24–32 km). This indicates somewhat continuous activity at this depth prior to the Mw 8.1 event on April 1, 2014. In future work, this observation may allow us to study the depths of foreshock activity and to identify possible precursor activity that could be used for earthquake early warning.

We selected series B to study the dynamic mutability within a time window of 64 events for different depth intervals (Fig. 7). Series B was selected over other time periods because the activity can be attributed solely to the earthquakes of March 2014. Between 12 and 18 km (Fig. 7a), aftershock activity is clearly observed after the earthquake of March 16 (i.e., falling mutability). Between 18 and 24 km (Fig. 7b), similar aftershock activity is clearly observed after the earthquake of March 16 (i.e., falling mutability), but a second set of reactions (a recovery and subsequent drop in mutability) is also observed. This signal

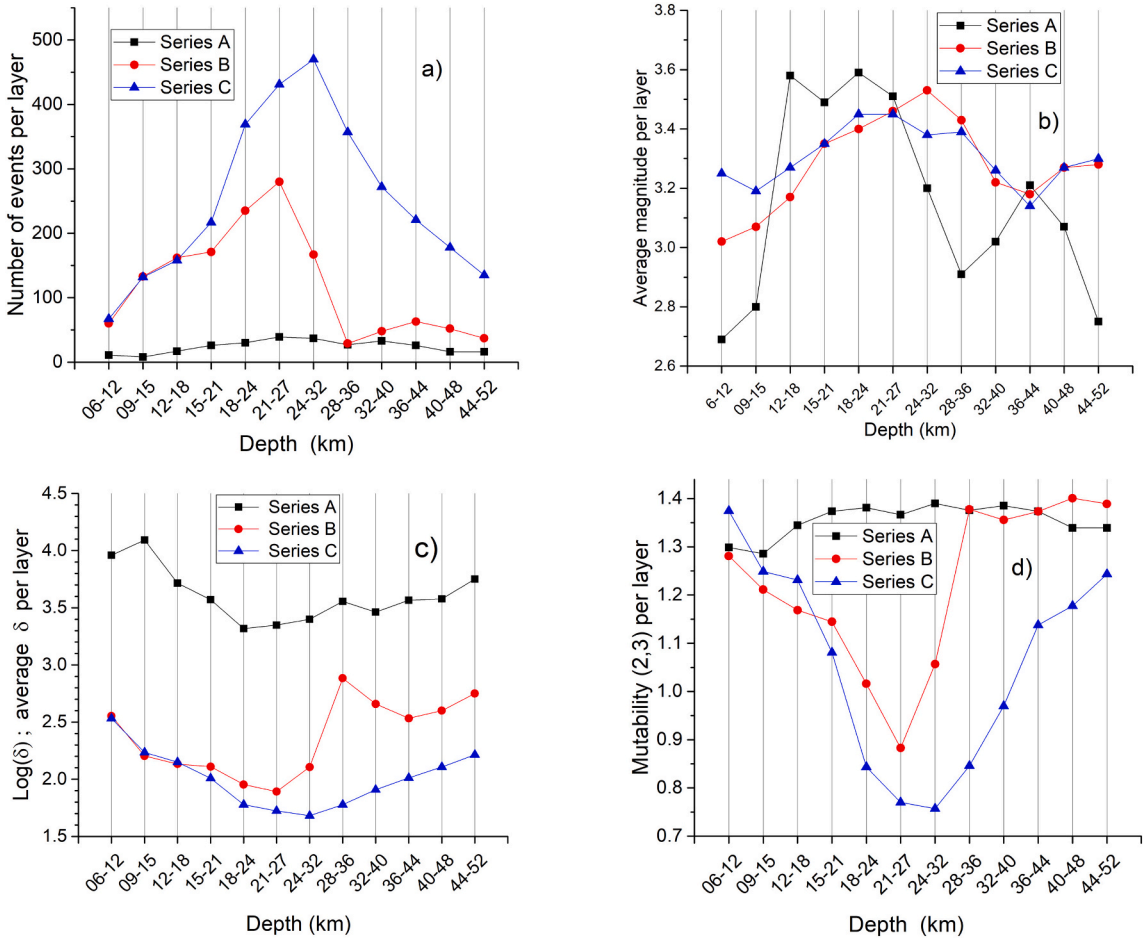

Fig. 5. Earthquake characteristics by depth interval for series A, B, and C. (a) Number of earthquakes per year. (b) Average magnitude per year. (c) Logarithm of the average interval ⟨δ⟩ in minutes between consecutive earthquakes. (d) Mutability per year.

relates to a Mw 6.4 earthquake with a depth of ~24 km on March 23, 2014. In contrast, the logarithm of the average interval ⟨δ⟩ in minutes between consecutive earthquakes (Fig. 5c) does not show evidence for the large, shallow earthquakes of early March; only the later and deeper earthquakes cause a fall in the mutability function. This clearly indicates the power of this technique for detecting local activity if a sequence of events can be produced for a given depth.

Since the IPOC database does not cover recent years, we also used the CSN catalog to investigate changes in mutability between 2012 and 2021 (Fig. 8). The absolute value of mutability depends on the density of data; therefore, results based on data from different sources and for different time periods are not directly comparable. However, the tendency of the mutability measured using the CSN data was found to be consistent with that for the same period using the IPOC data (Fig. 4), particularly with regards to the variation during 2014. Within a year of the 2014 activity, the mutability had recovered to the level seen before the large earthquakes.

An unexpected finding was that the dynamic average depth (calculated from the last 64 events) closely follows the mutability. Before the Mw 6.6 and 6.4 foreshocks of March 2014, the depth oscillated around 80 km as shown with respect to the right ordinate axis in Fig. 8. During and immediately after the March/April 2014 events, the average depth oscillated around 30 to 40 km. Afterwards, the average depth returned to ~80 km. However, the recovery rates (slopes in Fig. 8) for depth were slower than those for mutability.

Three significant earthquakes have occurred since April 2014: a M6.0 on June 19, 2014, a M6.3 on October 10, 2017, and a M6.3 on September 11, 2020. The first represents an important aftershock of series C. The second was deeper and produced a short-lived drop in mutability without altering the average depth. The third was at an intermediate depth and caused significant short-lived drops in both mutability and average depth, followed a gentler recovery of mutability to the long-term average, similar to the pattern observed for the earlier aftershock recoveries (see Fig. 4 and Vogel et al. [25]).

A number of additional observations require further investigation in the future. First, just before the initial earthquake of March 16, 2014 (at ~700 events), there was a small decrease in mutability, similar to the extended decreases of the aftershock regimes, and a small decrease in the average depth. Future work is needed to assess whether this signal is present before other large subduction earthquakes. Second, we observed that the average depth increased towards the end of 2021 (to between 100 and 110 km), while mutability remained stable slightly below the 2012–2013 average. The meaning of this behavior in terms of a potential megathrust event in this region remains unknown but could be interpreted as reflecting relaxation mechanisms that are postponing the expected megathrust event in this region.

5. Conclusions

The results of this study confirm that the content of the sequence of intervals between consecutive earthquakes, as recognized by mutability of appropriate precision [25–27,29], can recognize aftershocks regimes of different earthquakes and characterize their depth trends. Four major earthquakes near Iquique in 2014 occurred in pairs. The first couple, Mw 6.6 and 6.4 events, resulted in a shallow–deep aftershock regime during the second half of March 2014. Activity was initially focused in the

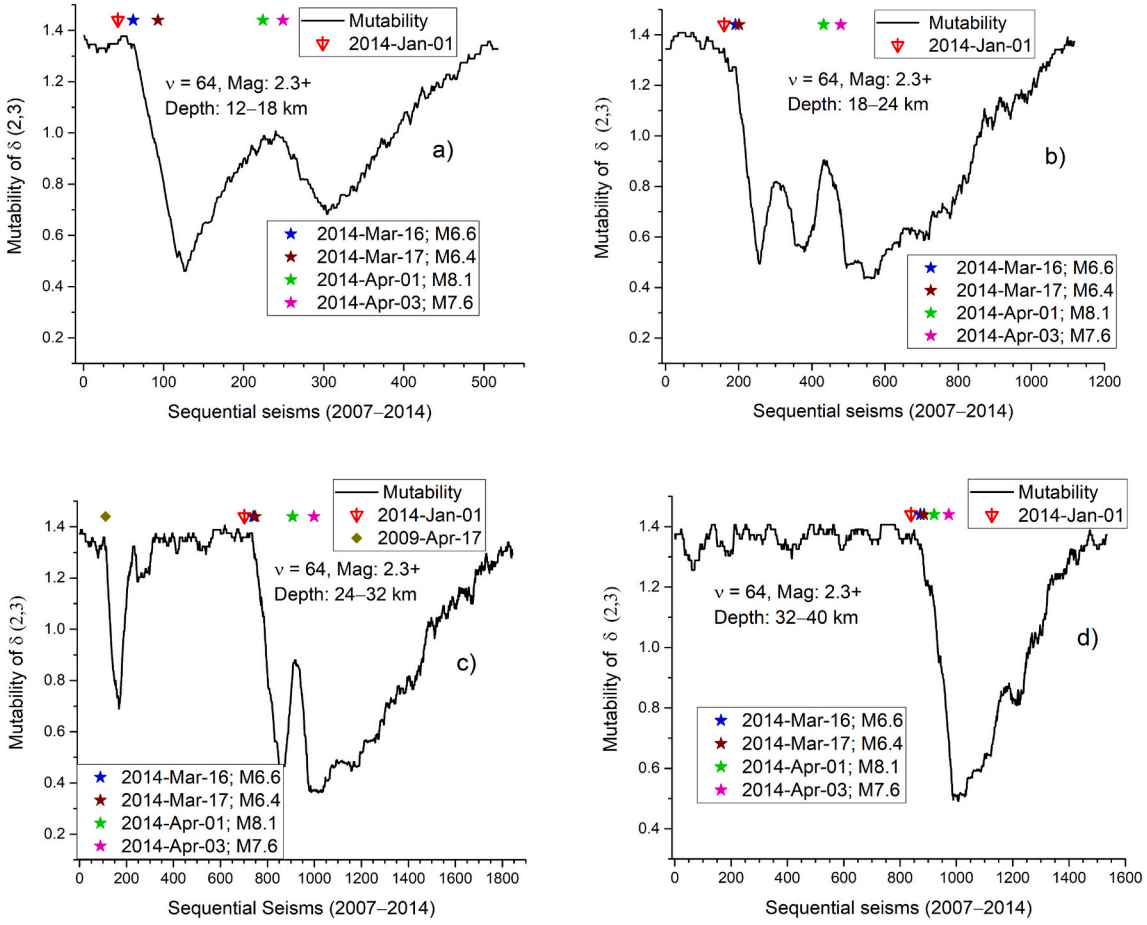

Fig. 6. Mutability of the δ function for different depth layers. (a) 12–18 km. (b) 18–24 km. (c) 24–32 km. (d) 32–40 km. The sequence of earthquakes (x axis) is not linear with time. The mutability (y axis) reflects the 64 most recent events corresponding to the indicated depth. The four most important earthquakes of the March/April 2014 period (as listed in Table I) are shown by star symbols. Other symbols denote other large earthquakes.

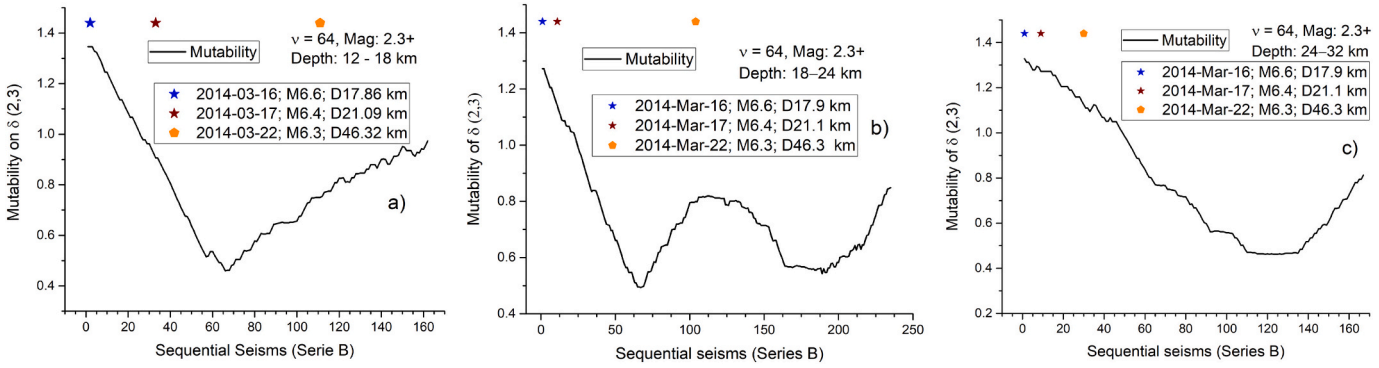

Fig. 7. Mutability of the δ function in different depth layers for series B. (a) 12–18 km. (b) 18–24 km. (c) 24–32 km. The three most important earthquakes are shown by star symbols.

12–18 km depth interval, but later increased to ~24 km depth. Within the, 18–24 km depth interval, we observed two sources of aftershock activity, which differed in both depth and time. We suggest that the second and deeper aftershock activity was related to a Mw 6.3 earthquake that occurred at a depth of 46.32 km, inside the Nazca plate (Table 1, Fig. 7). The second couple, Mw 8.1 and 7.6 events, were deeper and stronger than those of March 2014, and were separated by ~100 km in the north–south direction. Their aftershock regimes extended to ~50 km depth (see series C in Fig. 5); the events were concentrated during April 2014 but continued throughout 2014 with a decreasing trend. An earlier decrease in the mutability function during 2009 was related to a 27.2 km deep Mw 6.4 event on April 17. This was an isolated event that did not propagate or influence later aftershock activity.

The locations and depths of aftershocks are consistent with the subduction interface. Mutability values showed short-lived decreases within all depth intervals after the 2014 activity. At present, mutability levels are slightly below the pre-2014 average. Investigations of mutability during calm periods within different depth intervals could reveal "hidden" activity, but this is beyond the scope of the present study. It is possible that the slightly depressed mutability of recent years reflects

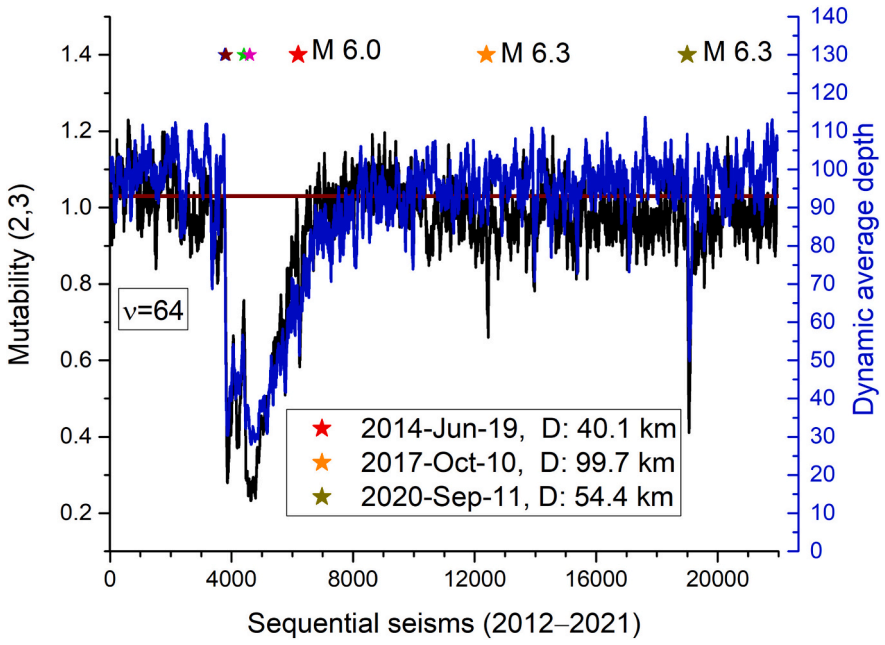

Fig. 8. Mutability and dynamical average depth of earthquakes for the earthquake sequence from 2012 to 2021. Smaller overlapping stars to the left denote 4 reference seisms during March and April 2014 (tabulated in boldface). Larger stars denote earthquakes with magnitude over 6.0 that occurred afterwards. The horizontal line corresponds to the average mutability over 2012 & 2013 (i.e., before the 2014 earthquakes). Data measured by the Centro Sismológico Nacional (CSN) of Chile.

relaxation mechanisms that are postponing the expected megathrust event in this region.

CRediT authorship contribution statement

E.E.V and D. P. conceived and designed the study. E.E.V. and G.S. carried out the statistical calculations. D.P. and A.P. formulated the geophysical framework of the work. All authors participated in the discussions, contributed to the analyses, wrote parts of the papers, prepared figures, and read and approved the final version of the paper.

Declaration of competing interest

The authors declare that they have no known competing financial interests or personal relationships that could have appeared to influence the work reported in this paper.

Data availability

Sippl, C., et al. (2018), GFZ Data Services, doi.org/10.5880/GFZ.4.1.2018.001 and CSN https://doi.org/10.7914/SN/C1

Acknowledgments

This work was supported by ANID (Chile) through Fondecyt (contract 1190036 to E.E.V.), the Center for Development of Nanoscience and Nanotechnology (CE-DENNA; contract AFB180001 to E.E.V.), and the RNM194 Research Groups of Junta de Andalucia, Spain (support provided to A.P.). Data were provided by the Integrated Plate Boundary Observatory Chile (IPOC) and the Centro Sismológico Nacional (CSN) of Chile.

Appendix 1

The choice of a time window with $\nu = 64$ is justified in Fig. A1, where two additional time windows are included (48 and 96). Evidently, $\nu = 64$ produces a wider response in mutability values during the aftershock regimes, which allows a better determination of differences. The depth bin between 21 and 27 km was chosen for this illustration, but similar plots have been obtained for other depths.

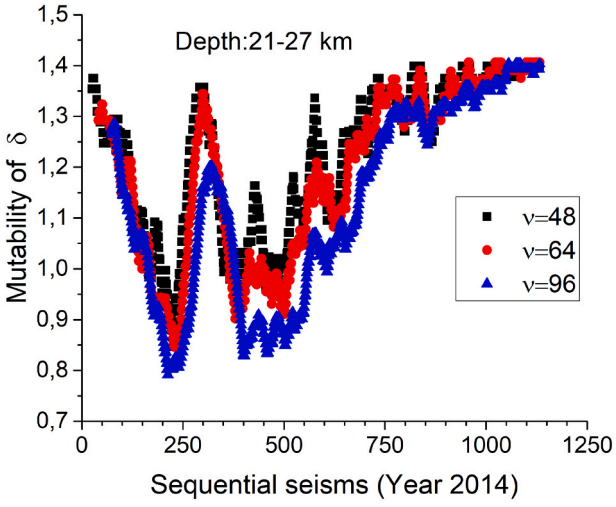

Fig. A1. Illustration of mutability for different time windows as shown in the inset.

The tuning of wlzip is illustrated in Fig. A2; four different truncation alternatives are shown for the same set of data (series B: all depths from April 1 to 142,014). Tuning of (2,3) renders the largest range, and hence offers better precision to characterize intermediate cases. Similar compression procedures were performed for the series (1,r) and (3,r) [data not shown], but tuning (2,3) had advantages over others and as such was chosen for use in this study.

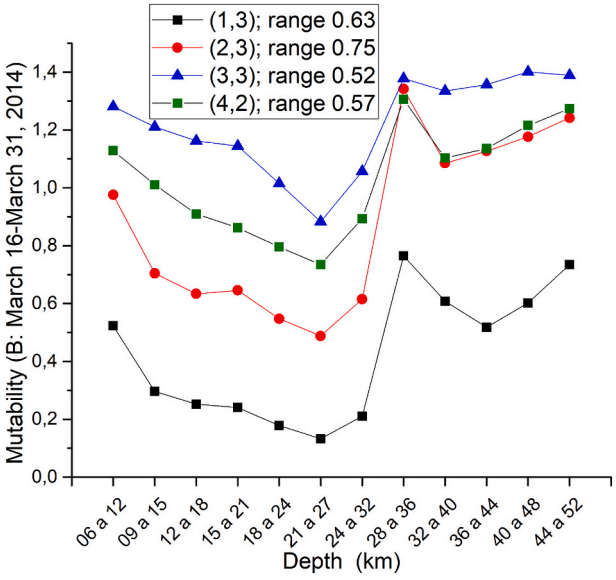

Fig. A2. Illustration of wlzip tuning. The data used in each curve is the same and corresponds to series B (see Section 2). The four data recognitions in the format (i,r) consider r digits, starting at position i. Setting the configuration to (2,3) produced the largest range in mutability, allowing for better classification of the property under study.

The results shown in Fig. 4 can also be represented in real time units from January 1, 2007, to December 312,014 (Fig. A3). The main difference is that events in the aftershock regime are more compressed, and so the texture of the sequence is somewhat lost. For this reason, our analysis was performed in terms of sequences of events, which made it easier to appreciate different important events during responses to the main earthquakes. One advantage of Fig. A3 is that a prominent drop in mutability can be seen for the Mw 6.3 earthquake of 2009 and its short aftershock period.

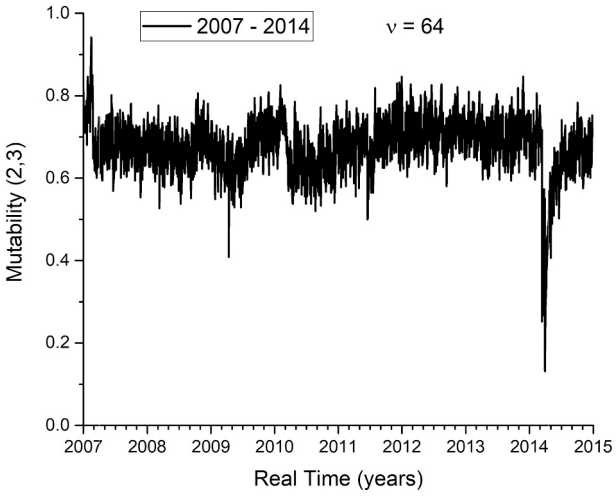

Fig. A3. Sequential earthquakes presented in real time with years as the main unit (in contrast to Fig. 4, where the x axis is not linear with time).

References

[1] Unnikrishnan K. Comparison of chaotic aspects of magnetosphere under various physical conditions using AE index time series. Ann Geophys 2008;26:941–53. https://doi.org/10.5194/angeo-26-941-2008.

[2] Berera A, Ho R. Chaotic properties of a turbulent isotropic fluid. Phys Rev Lett 2018;120(2):024101. https://doi.org/10.1103/PhysRevLett.120.024101.

[3] Dmitri V, Alexandrov IA, Bashkirtseva MC, Lev BR. Nonlinear climate dynamics: from deterministic behaviour to stochastic excitability and chaos. Phys Rep 2021; 902:1–60. https://doi.org/10.1016/j.physrep.2020.11.002.

[4] Lana X, Martínez MD, Posadas AM, Canas JA. Fractal behaviour of the seismicity in the southern Iberian Peninsula. Nonlinear Process. Geophys. 2005;12:353–61. https://doi.org/10.5194/npg-12-353-2005.

[5] Telesca L, Lapenna V, Lovallo M. Information entropy analysis of seismicity of Umbria-Marche region (Central Italy). Nat. Hazards Earth Syst. Sci. 2004;4:691–5. https://doi.org/10.5194/nhess-4-691-2004.

[6] Telesca L, Lovallo M, Mohamed AEA, ElGabry M, Elhady S, Abou Elenean KM, ElBary REF. Informational analysis of seismic sequences by applying the fisher information measure and the Shannon entropy: an application to the 2004–2010 seismicity of Aswan area (Egypt). Physica A 2012;391:2889–97.

[7] Telesca L, Lovallo M, Chamoli A, Dimri VP, Srivastava K. Fisher-Shannon analysis of seismograms of tsunamigenic and non-tsunamigenic earthquakes. Physica A 2013;392:3424–9.

[8] Telesca L, Lovallo M, Romano G, Konstantinou KI, Chen C-C, Hsu H-L. Using the informational Fisher-Shannon method to investigate the influence of long-term deformation processes on geoelectrical signals: an example from the Taiwan orogeny. Physica A 2014;414:340–51.

[9] Telesca L, Thai AT, Lovallo M, Cao DT, Nguyen LM. Shannon entropy analysis of reservoir-triggered seismicity at song tranh 2 hydropower plantVietnam. Appl. Sci 2022;12:8873. https://doi.org/10.3390/app12178873.

[10] Varotsos PA, Sarlis NV, Efthimios S, Skordas ES, Tanaka H. A plausible explanation of the b-value in the Gutenberg-Richter law from first principles. Proc. of the Japan Acad. Series B 2004;80(9):429–34.

[11] Varotsos PA, Sarlis NV, Skordas ES, Tanaka HK, Lazaridou MS. Attempt to distinguish long-range temporal correlations from the statistics of the increments by natural time analysis. Phys Rev E 2006;74:021123.

[12] Varotsos PA, Sarlis NV, Tanaka HK, Skordas ES. Similarity of fluctuations in correlated systems: the case of seismicity. Phys Rev E 2005;72:041103. https://doi.org/10.1103/PhysRevE.72.041103.

[13] Sarlis NV, Skordas ES, Varotsos PA. The change of the entropy in natural time under time-reversal in the Olami–Feder–Christensen earthquake model. Tectonophysics 2011;513(1):49–53.

[14] Sarlis NV, Skordas ES, Varotsos PA, Ramírez-Rojas A, Flores-Márquez EL. Natural time analysis: on the deadly Mexico M8.2earthquake on 7 September 2017. Physica A 2018;506:625–34.

[15] Rundle JB, Luginbuhl M, Giguere A, Turcotte DL. Natural time, nowcasting, and the physics of earthquakes: estimation ofseismic risk to global megacities. Pure Appl Geophys 2018;175:647–60. https://doi.org/10.1007/s00024-017-1720-x.

[16] Rundle JB, Giguere A, Turcotte DL, Donnellan A, Crutchfield JP. Global seismic nowcasting withShannon information entropy. Earthand Space Science 2019;6: 191–7.

[17] Hayes GP, Herman MW, Barnhart WD, Furlong KP, Riquelme S, Benz HM, et al. Continuing megathrust earthquake potential in Chile after the 2014 Iquique earthquake. Nature 2014;512(7514):295–8. https://doi.org/10.1038/nature13677.

[18] Ruiz S, Metois M, Fuenzalida A, Ruiz J, Leyton F, Grandin R, et al. Intense foreshocks and a slow slip event preceded the 2014 Iquique mw 8.1 earthquake. Science 2014;345(6201):1165–9. https://doi.org/10.1126/science.1256074.

[19] Schurr B, Asch G, Rosenau M, Wang R, Oncken O, Barrientos S, et al. The 2007 M7.7 Tocopilla northern Chile earthquake sequence: implications for along-strike and downdip rupture segmentation and megathrust frictional behavior. J Geophys Res 2012;117:B05305. https://doi.org/10.1029/2011JB009030.

[20] Ruiz S, Madariaga R. Historical and recent large megathrust earthquakes in Chile. Tectonophysics 2018;733:37–56. https://doi.org/10.1016/j.tecto.2018.01.015.

[21] Delouis B, Monfret T, Dorbath L, Pardo M, Rivera L, Comte D, et al. The Mw = 8.0 Antofagasta (Northern Chile) earthquake of 30 July 1995: a precursor to the end of the large 1877 gap. Bull Seismol Soc Am 1997;87(2):427–45.

[22] Tavera H, Fernández E, Bernal I, Antayhua Y, Agüero C, Salas H, et al. The southern region of Peru earthquake of June 23rd, 2001. J Seismol 2006;10:171–95. https://doi.org/10.1007/s10950-006-9014-2.

[23] León-Ríos S, Ruiz S, Maksymowicz A, Leyton F, Fuenzalida A, Madariaga R. Diversity of the 2014 Iquique's foreshocks and aftershocks: clues about the complex rupture process of a mw 8.1 earthquake. J Seismol 2016;20(4):1059–73. https://doi.org/10.1007/s10950-016-9568-6.

[24] Sippl C, Schurr B, Asch G, Kummerow J. Seismicity structure of the northern Chile forearc from >100,000 double-difference relocated hypocenters. J Geophys Res 2018;123(5):4063–87. https://doi.org/10.1002/2017JB015384.

[25] Vogel EE, Saravia G, Pasten D, Muñoz V. Time-series analysis of earthquake sequences by means of information recognizer. Tectonophysics 2017;712:723–8. https://doi.org/10.1016/j.tecto.2017.06.031.

[26] Vogel EE, Brevis FG, Pastén D, Muñoz V, Miranda RA, Chian ACL. Measuring the seismic risk along the Nazca-south american subduction front: Shannon entropy and mutability. Nat Hazard Earth Syst Sci 2020;20:2943–60. https://doi.org/10.5194/nhess-20-2943-2020.

[27] Vogel EE, Saravia G, Bachmann F, Fierro B, Fischer J. Phase transitions in Edwards-Anderson model by means of information theory. Phys A Stat Mech Appl 2009;388 (19):4075–82. https://doi.org/10.1016/j.physa.2009.06.010.

[28] Cortez V. Series de tiempo en vidrios de spin de tres dimensiones. Chile: Universidad de La Frontera; 2009. Ph.D Thesis.

[29] Vogel EE, Saravia G, Cortez LV. Data compressor designed to improve recognition of magnetic phases. Phys A Stat Mech Appl 2012;391(4):1591–601. https://doi.org/10.1016/j.physa.2011.09.005.

[30] Vogel EE, Saravia G. Information theory applied to econophysics: stock market behaviors. Eur Phys J 2014;B87(8):1–15. https://doi.org/10.1140/epjb/e2014-41003-0.

[31] Vogel EE, Saravia G, Astete J, Díaz J, Riadi F. Information theory as a tool to improve individual pensions: the chilean case. Phys A Stat Mech Appl 2015;424: 372–82. https://doi.org/10.1016/j.physa.2015.01.023.

[32] Contreras DJ. Diagnóstico de hipertensión arterial (HTA) a partir del análisis de holters mediante compresores de información. Thesis: Universidad de La Frontera, Chile; 2015.

[33] Contreras DJ, Vogel EE, Saravia G, Stockins B. Derivation of a measure of systolic blood pressure mutability: a novel information theory-based metric from ambulatory blood pressure tests. J Am Soc Hypertens 2016;10(3):217–23. https://doi.org/10.1016/j.jash.2015.12.010.

[34] Vogel EE, Saravia G, Ramirez-Pastor AJ. Phase transitions in a system of long rods on two-dimensional lattices by means of information theory. Phys Rev E 2017;96 (6):062133. https://doi.org/10.1103/PhysRevE.96.062133.

[35] Vogel EE, Saravia G, Kobe S, Schumann R, Schuster R. A novel method to optimize electricity generation from wind energy. Renew Energy 2018;126:724–35. https://doi.org/10.1016/j.renene.2018.03.064.

[36] Pasinetti PM, Ramirez-Pastor AJ, Vogel EE, Saravia G. Entropy-driven phases at high coverage adsorption of straight rigid rods on two-dimensional square lattices. Phys Rev E 2021;104, 5:054136. https://doi.org/10.1103/PhysRevE.104.054136.
[37] Métois M, Socquet A, Vigny C, Carrizo D, Peyrat S, Delorme A, et al. Revisiting the North Chile seismic gap segmentation using GPS-derived interseismic coupling. Geophys J Int 2013;194:1283–94. https://doi.org/10.1093/gji/ggt183.
[38] Metois M, Valderas-Bermejo C. GPS-derived interseismic coupling on the subduction and seismic hazards in the Atacama regionChile. Geophys J Int 2014; 196:644–55. https://doi.org/10.1093/gji/ggt418.
[39] Ruiz S, Klein E, del Campo F, Rivera E, Poli P, Metois M, Christophe V, Baez JC, Vargas G, Leyton F, Madariaga R, Fleitout L. The seismic sequence of the 16 september 2015 mw 8.3 Illapel, Chile, earthquake. Seismol Res Lett 2016;87(4): 789–99. https://doi.org/10.1785/0220150281.
[40] Wiemer S, Wyss M. Minimum magnitude of complete reporting in earthquake catalogs: examples from Alaska, the Western United States, and Japan. Bull Seismol Soc Am 2000;90:859–69. https://doi.org/10.1785/0119990114.
[41] Zúñiga F, Wyss M. Inadvertent changes in magnitude reported in earthquake catalogs: their evaluation through b-value estimates. Bull Seismol Soc Am 1995;85: 1858–66.
[42] Rydelek PA, Sacks IS. Testing the completeness of earthquake catalogs and the hypothesis of self-similarity. Nature 1989;337:251–3. https://doi.org/10.1038/337251a0.
[43] Ogata Y, Katsura K. Analysis of temporal and spatial heterogeneity of magnitude frequency distribution inferred from earthquake catalogues. Geophys J Int 1993;3 (113):727–38. https://doi.org/10.1111/j.1365-246X.1993.tb04663.x.
[44] Wiemer S, Wyss M. Minimum magnitude of complete reporting in earthquake catalogs: examples from Alaska, the Western United States, and Japan. Bull Seismol Soc Am 2000;90:859–69. https://doi.org/10.1785/0119990114.
[45] Cao AM, Gao SS. Temporal variations of seismic b-values beneath northeastern Japan island arc. Geophys Res Lett 2002;29(9):1334. https://doi.org/10.1029/2001GL013775.
[46] Amorèse D. Applying a change-point detection method on frequency-magnitude distributions. Bull Seismol Soc Am 2007;97:1742–9. https://doi.org/10.1785/0120060181.
[47] Mignan A, Woessner J. Estimating the magnitude of completeness for earthquake catalogs. In: Community Online Resource for Statistical Seismicity Analysis; 2012. https://doi.org/10.5078/corssa-00180805.
[48] Rydelek PA, Sacks IS. Testing the completeness of earthquake catalogs and the hypothesis of self-similarity. Nature 1989;337:251–3. https://doi.org/10.1038/337251a0.
[49] Woessner J, Wiemer S. Assessing the quality of earthquake catalogues: estimating the magnitude of completeness and its uncertainty. Bull Seismol Soc Am 2005;95: 684–98. https://doi.org/10.1785/012040007.
[50] Amorèse D. Applying a change-point detection method on frequency-magnitude distributions. Bull Seismol Soc Am 2007;97:1742–9. https://doi.org/10.1785/0120060181.
[51] Kvaerna T, Ringdal F. Seismic threshold monitoring for continuous assessment of global detection capability. Bull Seismol Soc Am 1999;89:946–59.
[52] Schorlemmer D, Woessner J. Probability of detecting an earthquake. Bull Seismol Soc Am 2008;98:2103–17. https://doi.org/10.1785/0120070105.
[53] D'Alessandro A, Luzio D, D'Anna G, Mangano G. Seismic network evaluation through simulation: an application to the Italian National Seismic Network. Bull Seismol Soc Am 2011;101:1213–32. https://doi.org/10.1785/0120100066.
[54] Zúñiga F, Wyss M. Inadvertent changes in magnitude reported in earthquake catalogs: their evaluation through b-value estimates. Bull Seismol Soc Am 1995;85: 1858–66.
[55] Ogata Y, Katsura K. Analysis of temporal and spatial heterogeneity of magnitude frequency distribution inferred from earthquake catalogues. Geophys J Int 1993;3 (113):727–38. https://doi.org/10.1111/j.1365-246X.1993.tb04663.x.
[56] Cao AM, Gao SS. Temporal variations of seismic b-values beneath northeastern Japan island arc. Geophys Res Lett 2002;29(9):1334. https://doi.org/10.1029/2001GL013775.